Direct profiling of breast cancer-derived extracellular vesicles using Pd-perovskite electrochemical biosensing platform

Ehsan Dezhakam[1], Balal Khalilzadeh[2,3]*, Abdolhossein Naseri[1]*, Reza Rahbarghazi[2,4], Elham Mahmoudi[5], Aligholi Niaei[5,6], Mahdi Mahdipour[2], Narges Mardi[7] and Ibrahim Isildak[8]

*Correspondence:
balalkhalilzadeh@gmail.com;
khalilzadehb@tbzmed.ac.ir;
ab.naseri@gmail.com

[1] Department of Analytical Chemistry, Faculty of Chemistry, University of Tabriz, Tabriz, Iran
[2] Stem Cell Research Center (SCRC), Tabriz University of Medical Sciences, Tabriz 51664-14766, Iran
[3] Hematology and Oncology Research Center, Tabriz University of Medical Sciences, Tabriz, Iran
[4] Department of Applied Cell Sciences, Faculty of Advanced Medical Sciences, Tabriz University of Medical Sciences, Tabriz, Iran
[5] Catalyst and Reactor Research Lab., Department of Chemical & Petroleum Engineering, University of Tabriz, Tabriz, Iran
[6] Department of Physics, Faculty of Science, University of Sakarya, Sakarya, Turkey
[7] Department of Medical Biotechnology, Faculty of Advanced Medical Sciences, Tabriz University of Medical Sciences, Tabriz, Iran
[8] Department of Bioengineering, Faculty of Chemistry-Metallurgy, Yildiz Technical University, 34220 Istanbul, Turkey

Abstract

Extracellular vesicles (EVs) harbor several signaling molecules to maintain intercellular communication. Based on the exosomal cargo type, metabolic, genomic, and proteomic status of parent cells can be investigated. Due to the existence of trivial levels of target molecules inside EVs, the application of accurate and sensitive detection methods is mandatory. Here, we used an electrochemical immunosensor using a biotinylated monoclonal CD63 antibody as the capturing element for the detection of EVs isolated from MDA-MB-231 cells and cancer patients. Simultaneously, breast cancer biomarker CA-15-3 was detected in isolated EVs using a sandwich method to increase specificity. Data indicated a linear dynamic range of 2000–10000 EVs/µL and a lower limit of quantification of 2000 EVs/µL. Based on data from real sample analysis, the levels of exosomal CA-15-3 can differ according to the severity and systemic content of this factor. Pd-perovskite-based immunosensor provides a platform for quick and in-depth analysis of EVs isolated for cancer cells.

Keywords: Breast cancer, Extracellular vesicles, Perovskite, Electrochemical, Biosensing

Introduction

Breast cancer is the most common type of cancer in females (DeSantis et al. 2014). Despite the existence of numerous treatment protocols (Mustacchi et al. 2015; Sonnenblick and Piccart 2015; Tangutoori et al. 2015), approximately one-third of cancer patients after diagnosis due to expansion and metastasis of tumor cells to other sites particularly the brain, etc. (Siegel et al. 2018; Kodack et al. 2015; Gerratana et al. 2015). Emerging data have confirmed that EVs play an important role in the growth and metastasis of breast cancer cells. These features make EVs a potential tool for theranostic purposes (Redig and McAllister 2013; Abbasi-Malati et al. 2024). Among different EVs released from the host cells, exosomes and microvesicles (MVs), are produced in large quantities by cancer cells and generate a premetastatic "niche" (Lee et al. 2011). Among different biomarkers used for breast cancer, CA-15-3, soluble forms of MUC-1 protein, is the most widely used serum marker in breast cancer patients. Monitoring of CA-15-3

is useful for therapy efficiency in patients with metastatic breast cancer. In the clinical setting, several serum markers, such as CEA, TPA, TPS, and the shed form of HER2, can be used for the detection and monitoring of breast cancer (Sturgeon et al. 2008; Molina et al. 1998, 2010, 1999; Sölétormos et al. 2004; Barak et al. 2004). Of note, these markers are superior to CA-15-3. However, the specificity and sensitivity are increased when serum levels of CA 15-3 followed for the detection of recurrent/metastatic breast cancer at the late stages (Duffy et al. 2010; Ryu et al. 2023).

To date, several detection methods, such as ELISA, real-time PCR analysis, radioimmunoassay, fluorescent spectroscopy, and histological-based examination, have been used extensively in human medicine to diagnose, monitor, and follow up cancer patients (Neagu et al. 2021). To this end, multiple diagnostic techniques are widely used in hospitals, such as X-ray, ultrasound-based imaging, and nuclear magnetic resonance (Graeser et al. 2021). Unfortunately, these methods usually are invasive and require expensive instruments or complex, labor-intensive protocols (Asleh et al. 2022). Regarding low sensitivity and meager reproducibility to detect the neoplastic cells in the early stages, the application of some of these approaches is limited (Constantin et al. 2022). These features increase the possibility of circulating cancer cells in the blood and the development of progressive metastatic foci in remote sites (Das et al. 2023). Therefore, there is a consensus about the advent of accurate detection methods with suitable selectivity, sensitivity, and rapidity in small-dimension settings (Fu and Ma 2020).

Electrochemical biosensors are the most widely used types of biosensors due to many advantages, including cost- and time-effectiveness, higher sensitivity, as well as low sample volume (Sohrabi et al. 2022a, b; Dezhakam et al. 2023). In recent years, electrochemical biosensors have been great alternatives for the detection/quantification of EVs in clinical samples (Dezhakam et al. 2022; Xu et al. 2020). EVs, ranging from 50 to 150 nm, are abundant in biofluids such as urine, blood, saliva, and cerebrospinal fluids (Anastasiadou and Slack 2014; Kowal et al. 2014; Mardi et al. 2023a). Emerging data point to the fact that cancer cell EVs can be used for early and non-invasive detection of cancer type and dynamic behavior of neoplastic cells (Mostafazadeh et al. 2022; Mardi et al. 2023b). Despite recent progress in the fabrication and application of electrochemical biosensing for EV analysis (Im et al. 2014; Stremersch et al. 2016; Wang et al. 2019; He et al. 2018), economic issues and lack of appropriate detection strategies limit their application for the analysis of EVs in real human samples (Doldán et al. 2016; Boriachek et al. 2019). Several research works have been reported in the past several years to measure exosomes derived from breast cancer using electrochemical techniques. For example, in a research work, a screen-printed electrode modified with extraavidin was used to screen breast cancer exosomes with detection limit of 4.7×10^5 exosomes/μL (Yadav et al. 2017). The basis of their measurement was the sandwiching of cancerous exosomes using anti-CD9 as a general antibody and anti-HER2 as a specific antibody. Looking at the currents obtained from the modified electrode, it can be seen that the application of a novel nanocomposite such as perovskite, which has noble metal nanoparticles in its structure, as a modifier of the electrode surface, greatly improves the signal. In addition, it increases the efficiency of the biosensor by reaching lower detection limits followed by high sensitivity and stable and reproducible results. In another study

reported by Moura et al., exosomes were preconcentrated from cell culture supernatants on magnetic particles modified with antibodies against general tetraspanins as well as cancer-specific receptors (Moura et al. 2020). This designed electrochemical sensor was able to reach the limit of detection of 10^5 exosomes/μL with anti-CD81 modified magnetic particles and labeling based on CD24 and CD340 as cancer-related biomarkers. Furthermore, in another study, exosomes were detected through the biomarker CD326 (EpCAM) and simultaneously through the enzymatic activity of alkaline phosphatase as a biomarker of carcinogenesis with limit of detection of 10^5 exosomes/μL (Moura et al. 2022). As expected, not using a nanocomposite as an electrode surface modifier will reduce the effective surface area and subsequently, decrease the sensitivity. Also, using CD24 and CD326 antibodies instead of more specific antibodies such as CA15-3 will reduce the selectivity of the proposed sensor to breast cancer-derived exosomes. As a correlate, these modalities must be rapid, simple, cost-effective, and specific in the detection of EVs from breast cancer cells.

Recently, perovskite-type oxides have attracted much interest for their potential applications, in biosensing due to their diverse physical properties and rich redox properties reflected in their chemistry (Wang et al. 2013a, 2017; Cai et al. 2014). Perovskites are oxides with the general formula ABO_3, where A and B are metal cations. In this formula, the metal cation A has a larger ionic radius than cation B. Moreover, A is coordinated 12-fold by oxygen anions, while B is coordinated sixfold. Several elements of the periodic table can be substituted at the positions of A and B, resulting in the formation of varied perovskite types with diverse applications (Dai et al. 2018; Pena and Fierro 2001; Tsvetkova and Kozhukharov 2009). These materials possess distinct crystal structures, electronic properties, oxide ion mobility, and adjustable oxygen content through compositional modifications (Wang et al. 2013a; Boubezari et al. 2021). These characteristics greatly improve their catalytic activity for oxidation and reduction processes (Nezhad et al. 2021; Thurner et al. 2022), as well as their performance in electrochemical applications such as water splitting reactions (Mahmoudi et al. 2023), supercapacitors (Ahangari et al. 2023), electrochemical sensors, and fuel cells (Pena and Fierro 2001; Lucas et al. 2009). In recent years, La-based inorganic nanomaterials such as perovskite-type $LaNiO_3$ oxide nanofibers (Wang et al. 2013b), $LaTiO_3–Ag_{0.1,0.2}$ nanomaterials (Wang et al. 2017; Jia et al. 2015), $LaNi_{0.5}Ti_{0.5}O_3$ (Wang et al. 2010), and $La_{0.66}Sr_{0.33}MnO_3$ (Luque et al. 2009) have been investigated to improve the catalytic performance of electrochemical sensors and to fabricate highly sensitive sensors. The combination of palladium (Pd) with perovskite materials results in a highly sensitive biosensing platform. Pd enhances the catalytic activity and electron transfer rate, while perovskite provides a robust and stable structure. This synergy leads to high sensitivity in detecting specific biomarkers present on extracellular vesicles, allowing precise profiling capabilities (Atta et al. 2019; Ekram et al. 2016).

In this study, a label-free electrochemical biosensor was fabricated using palladium-based perovskite for the detection of EVs derived from breast cancer MDA-MB-231 cells. Furthermore, the designed method was applied to distinguish normal and breast cancer sera using the exosomal content of the breast cancer cell marker namely CA-15-3 (Scheme 1).
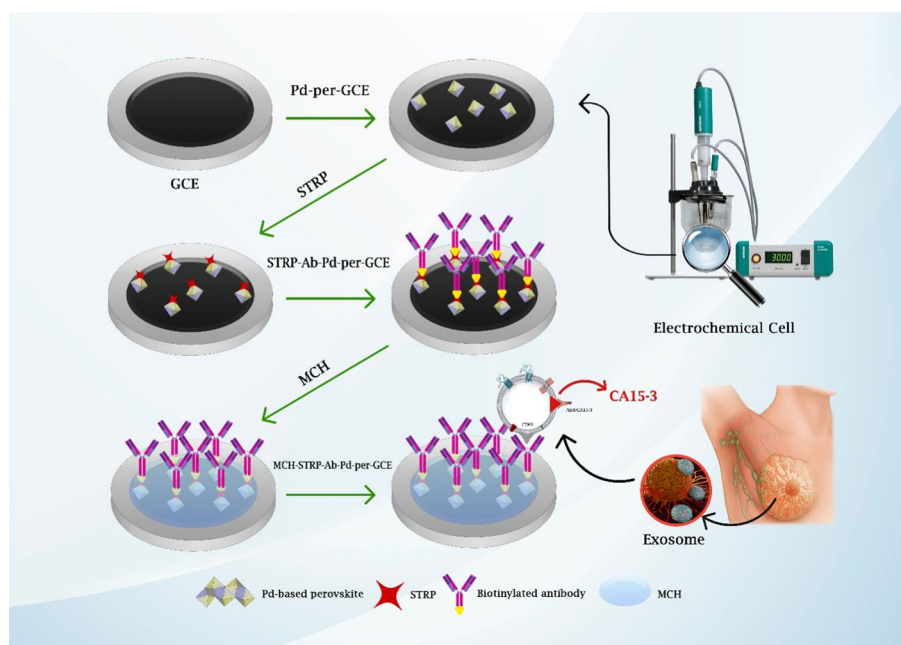
Scheme 1 Schematic presentation of developed biosensor

Material and methods

Materials

La $(NO_3)_3 \cdot 6H_2O$, Mn $(NO_3)_2 \cdot 4H_2O$, Fe $(NO_3)_3 \cdot 9H_2O$, Pd $(NO_3)_2 \cdot 2H_2O$, glycine, $NH_3 \cdot H_2O$ and 6-Mercaptohexanol (MCH) were obtained from Sigma-Aldrich. Biotinylated human monoclonal CD63 antibody and purified streptavidin protein were purchased from BioLegend Company. H_2SO_4, Na_2HPO_4, KH_2PO_4, KCl, $K_3[Fe(CN)_6]$, and $K_4[Fe(CN)_6]$ were obtained from Merck company.

Apparatus

All electrochemical measurements were recorded employing an Autolab 302N potentiostat/galvanostat electrochemical analyzer (Metrohm Co., Netherlands) proceeding by NOVA 2.1 software. The analysis system consisted of a three-electrode configuration including a working electrode (glassy carbon electrode, with 2 mm in diameter), a counter electrode (Pt wire), and a reference electrode (Ag/AgCl). An ultrasonic device (Strasonic 35) and a magnetic stirrer (Heidolph) were applied for the homogenization of the prepared solutions.

Characterization of nanomaterials

XRD

The crystalline phases of Pd/LaFe$_{0.7}$Mn$_{0.3}$O$_3$ were identified using X-ray diffraction analysis (XRD) with Cu-Kα radiation. Diffractograms were recorded with a step size of 0.02 degrees per 0.5 s for 2θ between 20° and 70°. Figure 1 shows the XRD pattern of as-prepared sample. The pattern indicates an orthorhombic structure, similar to that of
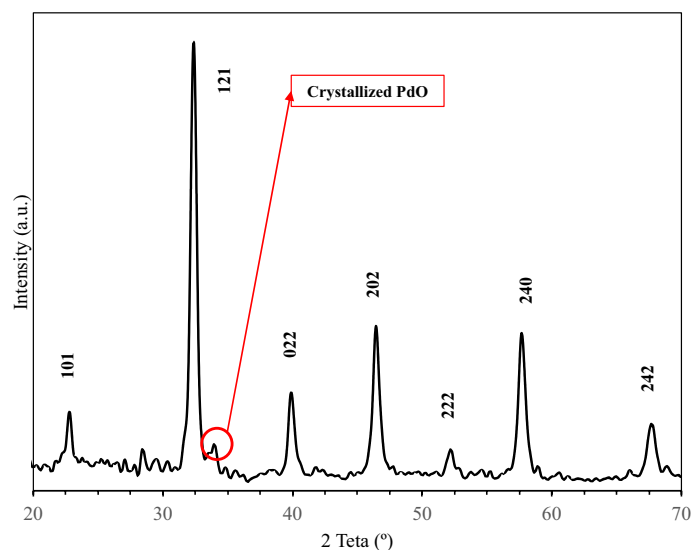
Dezhakam *et al. Cancer Nanotechnology*   (2024) 15:30

Page 5 of 16

Fig. 1 XRD profiles of synthesized $Pd_{0.1}/LaFe_{0.7}Mn_{0.3}O_3$

the cubic $LaFeO_3$ cubic perovskite (CSD 084941 card). Additionally, a small peak around 34.1° suggests the presence of a minor amount of PdO (Mohseni et al. 2024) on the surface of perovskite, consistent with the SEM results.

SEM

Samples were pre-coated with gold nanolayer, and their morphologies and the elemental composition were determined using Scanning Electron Microscopy instrument (SEM; MIRA3), and energy-dispersive X-ray (EDX) analysis on a Tescan instrument. The SEM images (Fig. 2a–c) reveal a porous morphology with perovskite pore size ranging from 557 to 627 nm, uniformly dispersed without sintering. Additionally, Pd particles are observed as an extra PdO phase within the perovskite structure, conforming the successful incorporation of Pd on the perovskite surface. The results of elemental composition using EDX analysis (Fig. 2d, e) aligns well with the calculated nominal values and XPS results, indicating successful Pd impregnation over the perovskite sample.

XPS

To evaluate the surface chemistry of the as-prepared $Pd_{0.1}/LaFe_{0.7}Mn_{0.3}O_3$ perovskite, XPS measurements were performed, with chemical shifts calibrated using C1s. Figure 3 shows the survey and elemental spectra results. Fe 2p spectra exhibit two prominent peaks at binding energies of 710.68 eV and 724.58 eV, corresponding to Fe $2p_{3/2}$ and Fe $2p_{1/2}$, respectively. In the Mn 2p spectra, the Mn $2p_{1/2}$ peak and Mn $2p_{3/2}$ peaks are located at 642.38 eV and 653.78 eV, respectively, with the Mn $2p_{3/2}$ peak indicating the presence of the Mn^{4+} component (Yoon et al. 2014). In the La 3d region, two double peaks were observed: one at lower binding energies (834.48 eV and 838.58 eV) corresponding to La $3d_{3/2}$ and La $3d_{5/2}$, and another at higher binding energies (851.48 and 855.48 eV) for La $3d_{3/2}$ (Redig and McAllister 2013). In the O1s region, two peaks were
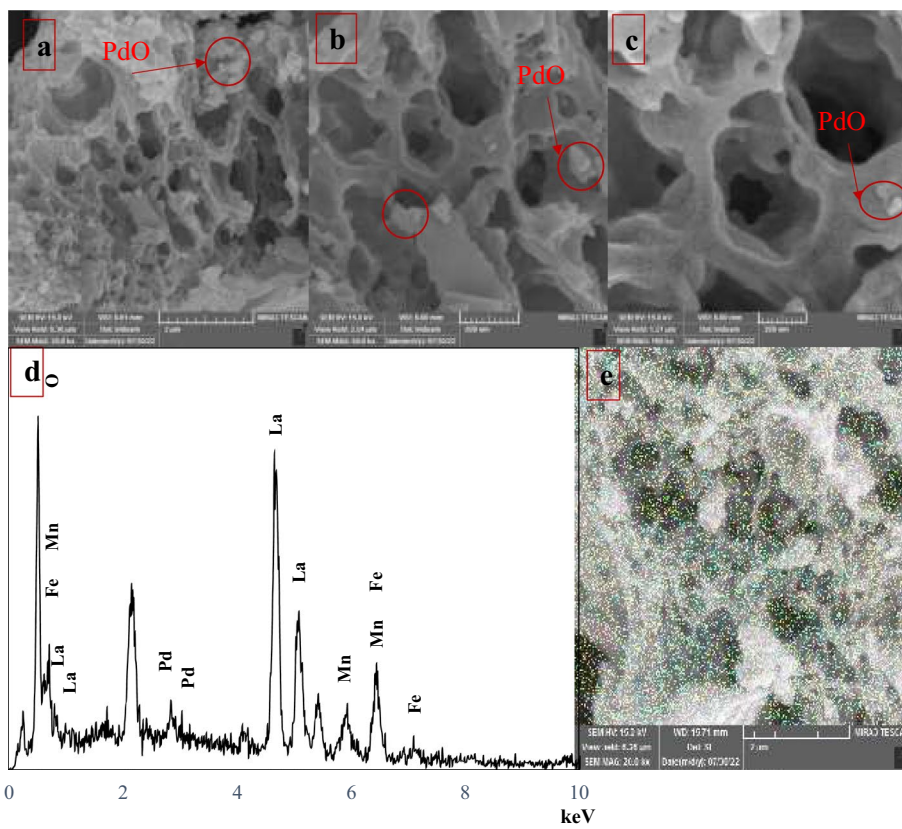
Dezhakam *et al. Cancer Nanotechnology*   (2024) 15:30

Page 6 of 16

Fig. 2 SEM (**a**–**c**) and EDS (**d**, **e**) results of $Pd_{0.1}/LaFe_{0.7}Mn_{0.3}O_3$
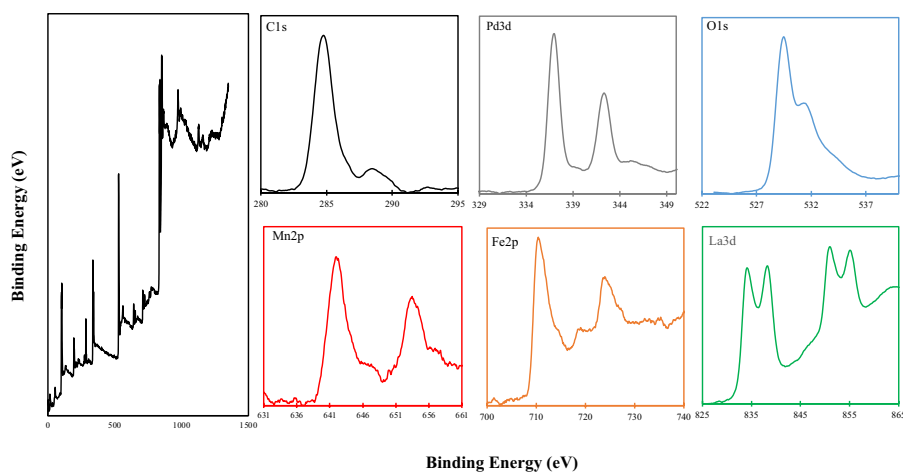

Fig. 3 XPS survey and elemental spectra of $Pd_{0.1}/LaFe_{0.7}Mn_{0.3}O_3$

observed; the first at 529.38 eV is attributed to lattice oxygen, and the second to surface oxygen.

The Pd 3d spectra confirm the presence of Pd in the samples with peaks at 337.08 eV and 342.58 eV. However, the peaks of Pd $3p_{3/2}$ (state PdO) and Pd $3p_{3/2}$ (state PdO_3) overlap with the O1s, complicating the chemical state analysis.

TEM

Transmission electron microscopy (TEM) was performed using the Hitachi HighTech HT7700 to complete the structural analysis. The TEM analysis of $Pd_{0.1}/LaFe_{0.7}Mn_{0.3}O_3$ is shown in Fig. 4. These images reveal the presence of perovskite structures with nonuniformly and randomly distributed PdO, which is consistent with the findings from SEM and XRD analysis.

Synthesis of Pd-perovskite

$LaFe_{0.7}Mn_{0.3}O_3$ nanoparticles (NPs) were synthesized using the sol–gel method (Hosseini et al. 2018). $La(NO_3)_3 \cdot 6H_2O$, $Mn(NO_3)_2 \cdot 4H_2O$, and $Fe(NO_3)_3 \cdot 9H_2O$ were dissolved in de-ionized water in stoichiometric amounts and heated to 85 °C until a clear solution was obtained. Glycine was then added to the solution, and the pH was adjusted using $NH_3 \cdot H_2O$. After 2 h, the resulting gel was placed in an oven and heated to 350 °C until it burned to form a blackish-brown powder. This powder was then calcined at 700 °C for 5 h. For the synthesis of $Pd/LaFe_{0.7}Mn_{0.3}O_3$, the wet impregnation method was employed. Stoichiometric amounts of $Pd(NO_3)_2 \cdot 2H_2O$ and the perovskite were used to achieve a 10 wt% Pd loading relative to the perovskite. The mixture was dissolved in de-ionized water and stirred for 2 h, after which the temperature was increased to 70 °C to evaporate all the water. The resulting powder was then calcined at 600 °C for 5 h (Mohammadi et al. 2022).

Immobilization of Pd-perovskite on the glassy carbon electrode

The perovskite suspension was produced via a milling process and then dispersing 0.03 g Pd-perovskite powder in 10 mL distilled water. Next, the obtained suspension was placed in the ultrasonic device to disperse NPs for 2 h. Then, 2 mL of dispersed suspension and 8 mL of 0.1 M KCl were mixed and used for the electrodeposition of Pd-perovskite through the chronoamperometry (CHA) technique. In this way, 10 mL of
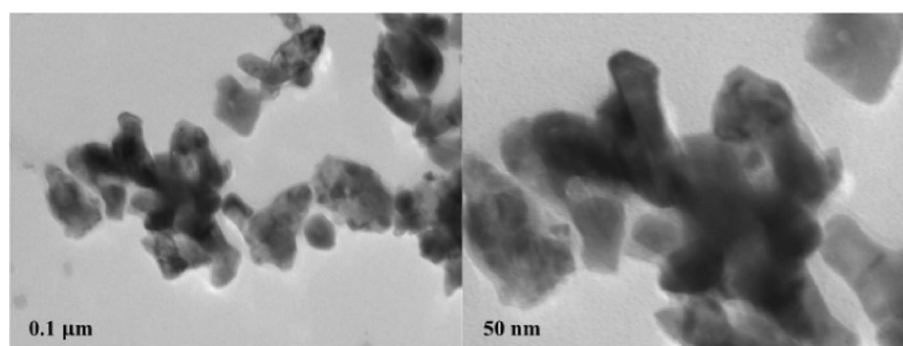

Fig. 4 TEM analysis of $Pd_{0.1}/LaFe_{0.7}Mn_{0.3}O_3$

the obtained solution was transferred to the electrochemical cell. The deposition process was carried out using the CHA technique ($P = -2.4$ V, $t = 30$ s). Afterward, the modified electrode was used for several analyses (Pd-per-GCE).

Optimization of the electrodeposition process

Deposition potential and time

To improve the sensitivity of the immunosensor, the active sites were promoted to increase the loading density of the capture (a relevant antibody). For this purpose, the thickness of perovskite on the surface of the electrode was optimized using the CHA technique. In this regard, the parameters of potential and time were optimized and the results were measured using square-wave voltammetry (SWV) in 5 mM $[Fe(CN)_6]^{3-/4-}$/0.1 M KCl (pH 7.4) solution as a standard of the electrochemical redox system. Supplementary Figure S1 panels A and B show the potential value of the solution was between -2.2 and -2.7 V. The potential value of -2.4 V was selected as optimal for the next analyses. One reason for the selection of this range of potentials would be the reduction potentials related to metals forming perovskite (Nasrollahpour et al. 2021). It should be noted that palladium can be lost probably at high potentials when it sweeps toward positive potentials. Thus, the current can be decreased because palladium is an active compound in this analytical approach. A short-duration event (30 s) with the simultaneous high current was selected (Supplementary Figure S1 panel C and D).

Immobilization of CD63 antibody on the Pd-perovskite-modified electrodes

1.5 µL of streptavidin (STRP, 1 µg mL^{-1}) was placed on the Pd-per-GCE. STRP was used to increase the loading capacity of CD63 antibody immobilization. It was suggested that STRP can provide more binding sites due to the unique molecular structure (Zhu et al. 2015), in which the sensitivity of the developed immunosensor can be theoretically enhanced four times. Following, 5 µL of CD63 antibody (1 µg mL^{-1}) was incubated for 90 min at 4 °C, followed by blocking with 2 µL of 1 mM MCH solution at 4 °C for 60 min. MCH was used to block the remaining active sites of the STRP-CD63-Pd-per-GCE surface to avoid non-specific adsorption (Li et al. 2018). In the final step, the STRP-CD63-MCH-Pd-per-GCE was employed as a sensitive and specific platform for capturing and detecting breast cancer EVs.

Optimization of STRP-related concentration, temperature, and time

It is believed that various parameters, such as concentration, incubation temperature, and time of STRP, can affect for site-specific loading of the anti-CD63 antibody (Nasrollahpour et al. 2023). In this regard, the optimization examinations were performed in 5 mM $[Fe(CN)_6]^{3-/4-}$/0.1 M KCl (pH 7.4) solution using the DPV technique. To evaluate the effect of STRP concentration on the Pd-per-GCE surface, the volume ranges of 1–6 µL were selected. As shown in Supplementary Figure S2 panels A and B, the recorded electrical signal remained almost constant according to values from 1 to 1.5 µL, and then gradually decreased at higher volumes. This is because STRP is an insulator and increasing its amount will decrease the electrical current of the modified electrode surface. Considering these results, the volume of 1.5 µL was selected for other optimization experiments. By analysis of different incubation temperatures (4, 25, and

37 °C), the developed immunosensor displayed a desirable response at 4 °C, and a further increase in temperature resulted in an unstable response (Supplementary Figure S2 panel C and D) (Zhu et al. 2015). Therefore, the temperature of 4 °C was considered the optimal incubation temperature of STRP for the immunosensing approach. The incubation time diagram on immunosensor performance is shown in Supplementary Figure S2 panels E and F. By increasing the incubation time up to 90 min, the recorded electrical current increases and decreases, respectively. With increasing incubation time after 90 min, approximately no changes were observed in the electrical current. Therefore, the time 90 min was selected as the optimal incubation time for STRP-Pd-per-GCE.

Optimization of antibody immobilization

For increasing the active site availability for improving the capturing efficiency of EVs, different experimental conditions such as concentration, incubation time, and temperature of biotinylated CD63 antibody were optimized. For this aim, optimization experiments were performed using the DPV technique in 5 mM $[Fe(CN)_6]^{3-/4-}$/0.1 M KCl (pH 7.4) solution. To investigate the effect of CD63 concentration, the drop volume ranges were chosen from 1 to 8 µL (Supplementary Figure S3 panels A and B). Due to the non-electroactivity feature of the antibody, the height of the recorded peaks decreases with the increase in the amount of CD63 antibody. Considering these results, the volume of 5 µL was chosen as optimal, because, in this amount of antibody, almost the STRP level of the antibody was conjugated. Regarding the optimization of the incubation temperature, by examining various incubation temperatures (4, 25, and 37 °C), the prepared immunosensor showed a favorable response at 4 °C, and increasing the temperature led to a significant decrease in electrical signals. Based on Supplementary Figure S3 panels C and D, the temperature 4 °C was considered as the optimal incubation temperature of anti-CD63 antibody for the biosensing approach. To optimize the incubation time, as presented in (Supplementary Figure S3 panels E and F), the time of 90 min was chosen optimally owing to having the best interaction between antibody and streptavidin performed.

Cell culture protocol

In this study, human breast cancer cell line MDA-MB-231 cells were purchased from the National Iranian Cell Bank (Pasteur Institute, Tehran). Cells were cultured in RPMI-1640 culture medium (Gibco) containing 10% fetal bovine serum (FBS) and 1% Pen-Strep. Culture flasks were maintained in standard conditions (37 °C, 95% relative humidity, and 5% CO_2). The culture medium was renewed every 3–4 days and cells sub-cultured at 70–80% confluence using 0.25% Trypsin–EDTA solution.

EVs isolation and purification

Cells between passages 3–6 were used for EV isolation. In short, MDA-MB-231 cells were incubated in a culture medium with 1% bovine serum albumin (Sigma-Aldrich) for 48 h. After that, the supernatant was collected and centrifuged at $300 \times g$ for 5 min to exclude the cells (Mobarak et al. 2021). The procedure followed by the centrifugation of supernatants at $2000 \times g$ (10 min), and $10,000 \times g$ (30 min) to remove cell debris contamination. Upon passing the samples through 0.22-µm-sized microfilters, EVs were

collected using Optima™ TLX-120 ultracentrifuge at 100,000×*g* for 60 min (Beckman Coulter Inc.). All centrifugation procedures were done at 4 °C. Samples were kept at −80 °C until the analyses.

Real sample collection

To examine the validity of the designed biosensor for the evaluation of breast cancer EVs, we collected sera from three breast cancer patients with different stages of anaplastic changes after the completion of informed consent. Tumor marker CA-15-3 levels were measured using a commercial immunoassay kit (ab108633). About 2 mL of blood samples were centrifuged at 2500 rpm for 10–15 min to collect serum. To measure CA-15-3 levels, 50 μL of samples were mixed in solutions A and B and read using the IMMULITE 2000 system (Siemens, Germany) and obtained data compared to the standard values. The remnants of samples were subjected to EV isolation using the above-mentioned protocol. It should be noted that in the next steps, we will generalize the results of this study to more patients. All phases of studies were approved by the National Institute of Medical Research Development (NIMAD). EVs were collected from samples as above-mentioned.

Statistical analysis

In this study, data are expressed as mean ± SD. To compare statistical differences between the groups, One-Way ANOVA with post hoc analysis was used. $P < 0.05$ was considered statistically significant.

Results and discussion

Calibration curve

After optimizing the experimental parameters, the developed immunosensor was used to examine different concentrations of EVs. In this regard, a semi-quantitative test was performed on the EVs that were previously isolated with the approximate number in certain volumes. Therefore, different volumes were properly immobilized on the designed immunosensor and their corresponding electrical currents were recorded by a sensitive
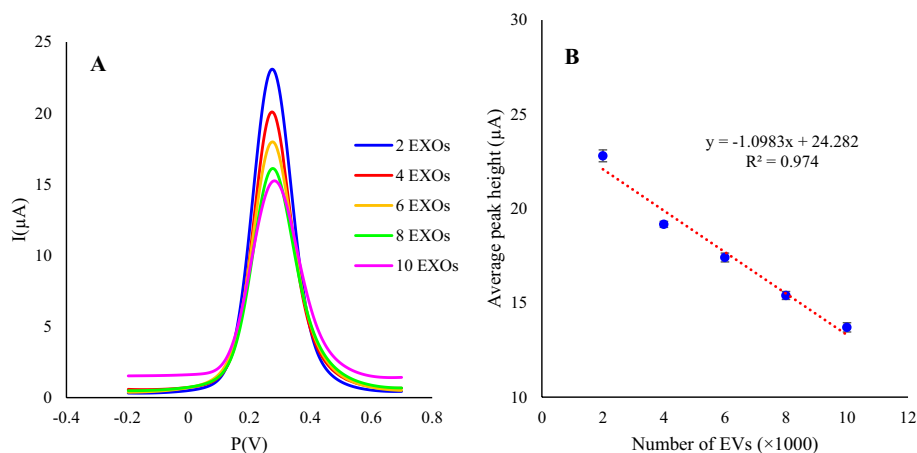

Fig. 5 A DPV signal readouts (number of EVs × 1000) and **B** calibration curve for different numbers of the EVs

technique (DPV) in 5 mM $[Fe(CN)_6]^{3-/4-}$/0.1 M KCl (pH 7.4) solution (Fig. 5). As shown in Fig. 5, the relationship between the recorded electrical current and the number of EVs is linear with a lower limit of quantification (LLOQ) of 2000 EVs/µL. It was notified that the linear dynamic range (LDR) is 2000 to 10,000 EVs/µL. Based on the results of a calibration curve, $Y = -1.0983x + 24.282$ and $R^2 = 0.974$ were obtained. In Fig. 5A, B represent the related voltammograms and average electrical current versus the number of EVs.

Preparation steps of biosensor

To improve the conductivity and increase the dense load of the capture element (anti-CD63), the surface of the glassy carbon electrode was modified using a Pd-based perovskite nanocomposite. According to Fig. 6, the modified electrode had approximately near twofold current than the bare electrode, indicating an improved efficiency of the designed immunosensor. These features can lead to efficient detection and sensitive analytical ranges for EVs. Streptavidin was used to increase the loading capacity of specific binding sites for biotinylated CD63 antibody. Data indicated that the reduced electrical current results from appropriate anti-CD63 antibody loading on the modified electrode. Anti-CD63 antibody was used as a capture element to provide active bioconjugation sites for the entrapment of EVs. Since covalently attached antibodies exhibit non-electroactive features, and thus, the height of the recorded peaks decreases after its immobilization. Using MCH, the remaining active sites from STRP-anti-CD63-Pd-per-GCE surface were blocked to prevent non-specific adsorption, which caused a slight decrease in the recorded signals. These data show the eligibility of designed sensor for the analysis of EVs.

Repeatability and reproducibility

The repeatability of the designed immunosensor was evaluated for the concentrations of 2000, 6000, and 10,000 EVs/µL, and favorable related standard deviations (RSD) for 10 repeated measurements were calculated to be about 1.38, 1.35, and 1.79%, respectively. This acceptable repeatability is due to the excellent electrochemical deposition of Pd-per on the GCE as well as the good interaction between the STRP and modified electrode, SRTP, biotin and finally capture element (antibody) and the EVs on the surface of the modified electrode. Also, the reproducibility of this proposed immunosensor is conducted by detecting EVs at the concentration of 6000 EVs/µL. The RSD of four immunosensors prepared in the same manner is 1.17%, showing a desirable reproducibility of this immunosensor for biomedical applications.

Real sample collection

Using ELISA, we noted higher serum levels of tumor marker CA-15-3 in females suffering breast cancer at different stages related to a healthy woman (Fig. 7A). Based on our data, tumor marker CA-15-3 ranged between 28.87 and 126 U/mL in 3 female patients compared to the normal level (12.7 U/mL). It was suggested that serum levels of CA-15-3 are closely related to initial primary tumor size and higher CA-15-3 levels are due to metabolically active lesions (Fakhari et al. 2019). It is postulated that the increase of exosomal CA-15-3 can reflect real-time metabolic in breast
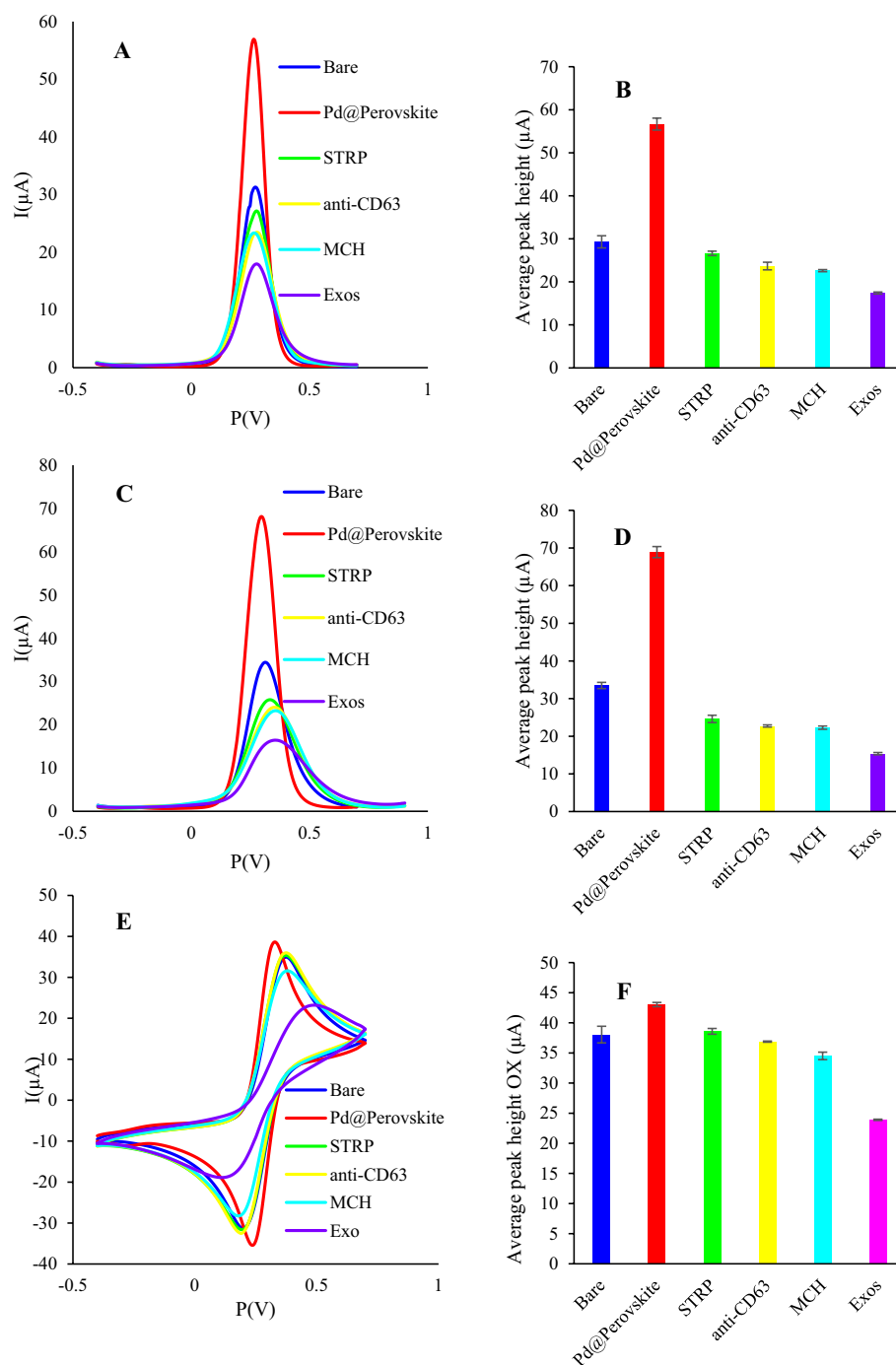
Fig. 6 Electrode preparation steps: DPV signals (**A**) and its related histogram (**B**). SWV signals (**C**) and related histogram (**D**). CV signals (**E**) and related histogram (**F**). All experiments were performed in 5 mM $[Fe(CN)_6]^{3-/4-}$/0.1 M KCl (pH 7.4) solution

cancer cells and progressive anaplastic changes with the possibility of metastasis to the ectopic sites (He et al. 2016). To examine whether breast cancer EVs can harbor CA-15-3 marker and find any changes in exosomal levels of CA-15-3 in patients at different stages, isolated control, and cancer EVs were exposed to the designed
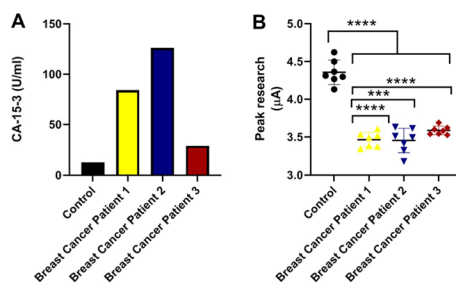
Fig. 7 Monitoring the levels of CA-15-3 using ELISA in breast cancer patient's sera compared to healthy counterparts (**A**). Detecting the exosomal levels of CA-15-3 in breast cancer patient's sera using a developed biosensor related to the control sample (**B**). Data indicated a proportional correlation between exosomal CA-15-3 levels and the stage of breast cancer analyzed by the developed biosensor. One-way ANOVA with Tukey post hoc analysis. ***$p < 0.001$; and ****$p < 0.0001$

STRP-anti-CD63-MCH-Pd-per-GCE platform and sandwiched with FDA approved anti-CA-15-3 antibody. The electrical currents of CA-15-3 modified electrodes were recorded as same as the calibration curve and the interesting and desirable results were recorded. Data indicated statistically significant differences in terms of electrical current between the control EVs with breast cancer EVs ($p < 0.0001$; Fig. 7B) in which the attachment of anti-CA-15-3 antibody to captured EVs led to lower electrical current (μA) values. Interestingly, we found that in breast cancer patient 1 with higher CA-15-3 levels, minimum electrical current was achieved (3.13 ± 0.04 μA) in comparison with other cancer EVs ($p < 0.05$; Fig. 7B). No statistically significant differences were found in electrical current between the groups with serum levels of CA-15-3 at ranges between 28.87 and 126 U/mL ($p > 0.05$). To be specific, these data demonstrated that EVs are valid bioshuttles to carry breast cancer CA-15-3 marker, and exosomal level changes were associated with serum levels of this factor and the progression of cancer cells within the mammary glands. Close changes in serum levels of CA-15-3 did not yield significant electrical current values.

Conclusion

In this study, an electrochemical assay was successfully designed to analyze breast cancer EVs. For this purpose, Pb-based perovskite nanostructures were synthesized as modifier nanomaterials with high conductivity, biocompatible, and cost-effectiveness. Perovskite nanocomposite was used to increase the electrode active area as well as effectively stabilize streptavidin and then the antibody on the surface of the modified electrode. The palladium presence in the perovskite structure as an active compound increases the active sites and the result of this simultaneously improves the stability and sensitivity of the designed immunosensor. In this regard, a redox $[Fe(CN)_6]^{3-/4-}$ system was implemented as a way to generate electrical current. The detection method is based on the specific binding of monoclonal anti-CD63 and anti-CA-15-3 to extracellular vesicles via sandwiching route for the screening of cancerous extracellular vesicles. To achieve the best results, all effective experimental conditions were optimized.

Supplementary Information

The online version contains supplementary material available at https://doi.org/10.1186/s12645-024-00270-6.

> Supplementary Material 1.

Availability of data and materials
Not applicable.

Declarations

Ethics approval and consent to participate
All procedures of this study were approved by the National Institute of Medical Research Development (NIMAD) (IR.NIMAD.REC.1400.125). All procedures were done in accordance with the Declaration of Helsinki.

Consent for publication
Not applicable.

Competing interests
The authors declare no competing interests.

References

Abbasi-Malati Z, Azizi SG, Milani SZ, Serej ZA, Mardi N, Amiri Z, Sanaat Z, Rahbarghazi R (2024) Tumorigenic and tumoricidal properties of exosomes in cancers; a forward look. Cell Commun Signal 22(1):130. https://doi.org/10.1186/s12964-024-01510-3

Ahangari M, Mostafaei J, Zakerifar H, Sayyah A, Delibaş N, Çoruh A, Mahmoudi E, Asghari E, Niaei A (2023) Effect of Pd doping on the structural properties and supercapacitor performance of La0. 8Sr0. 2Cu0. 7Mn0. 3O3 and La0. 8Sr0. 2Cu0. 4Mn0. 6O3 as electrode materials. Electrochim Acta 470:143274

Anastasiadou E, Slack FJ (2014) Malicious exosomes. Science 346(6216):1459–1460

Asleh K, Negri GL, Spencer Miko SE, Colborne S, Hughes CS, Wang XQ, Gao D, Gilks CB, Chia SK, Nielsen TO (2022) Proteomic analysis of archival breast cancer clinical specimens identifies biological subtypes with distinct survival outcomes. Nat Commun 13(1):896

Atta NF, Galal A, Ekram H (2019) Effect of B-site doping on Sr_2PdO_3 perovskite catalyst activity for non-enzymatic determination of glucose in biological fluids. J Electroanal Chem 852:113523

Barak V, Goike H, Panaretakis KW, Einarsson R (2004) Clinical utility of cytokeratins as tumor markers. Clin Biochem 37(7):529–540

Boriachek K, Masud MK, Palma C, Phan H-P, Yamauchi Y, Hossain MSA, Nguyen N-T, Salomon C, Shiddiky MJ (2019) Avoiding pre-isolation step in exosome analysis: direct isolation and sensitive detection of exosomes using gold-loaded nanoporous ferric oxide nanozymes. Anal Chem 91(6):3827–3834

Boubezari I, Zazoua A, Errachid A, Jaffrezic-Renault N (2021) Sensitive electrochemical detection of bioactive molecules (hydrogen peroxide, glucose, dopamine) with perovskites-based sensors. Chemosensors 9(10):289

Cai B, Zhao M, Wang Y, Zhou Y, Cai H, Ye Z, Huang J (2014) A perovskite-type KNbO3 nanoneedles based biosensor for direct electrochemistry of hydrogen peroxide. Ceram Int 40(6):8111–8116

Constantin N, Sina AAI, Korbie D, Trau M (2022) Opportunities for early cancer detection: the rise of ctDNA methylation-based pan-cancer screening technologies. Epigenomes 6(1):6

Dai H, Zhong Y, Wu X, Hu R, Wang L, Zhang Y, Fan G, Hu X, Li J, Yang Z (2018) Synthesis of perovskite-type $SrTiO_3$ nanoparticles for sensitive electrochemical biosensing applications. J Electroanal Chem 810:95–99

Das U, Banik S, Nadumane SS, Chakrabarti S, Gopal D, Kabekkodu SP, Srisungsitthisunti P, Mazumder N, Biswas R (2023) Isolation, detection and analysis of circulating tumour cells: a nanotechnological bioscope. Pharmaceutics 15(1):280

DeSantis CE, Lin CC, Mariotto AB, Siegel RL, Stein KD, Kramer JL, Alteri R, Robbins AS, Jemal A (2014) Cancer treatment and survivorship statistics, 2014. CA Cancer J Clin 64(4):252–271

Dezhakam E, Khalilzadeh B, Mahdipour M, Isildak I, Yousefi H, Ahmadi M, Naseri A, Rahbarghazi R (2022) Electrochemical biosensors in exosome analysis; a short journey to the present and future trends in early-stage evaluation of cancers. Biosens Bioelectron 222:114980

Dezhakam E, Tavakkol M, Kafili T, Nozohouri E, Naseri A, Khalilzadeh B, Rahbarghazi R (2023) Electrochemical and optical (bio) sensors for analysis of antibiotic residuals. Food Chem 439:138145

Doldán X, Fagúndez P, Cayota A, Laíz J, Tosar JP (2016) Electrochemical sandwich immunosensor for determination of exosomes based on surface marker-mediated signal amplification. Anal Chem 88(21):10466–10473

Duffy MJ, Evoy D, McDermott EW (2010) CA 15-3: uses and limitation as a biomarker for breast cancer. Clin Chim Acta 411(23–24):1869–1874

Ekram H, Galal A, Atta NF (2016) The effect of A-site doping in a strontium palladium perovskite and its applications for non-enzymatic glucose sensing. RSC Adv 6(20):16183–16196

Fakhari A, Gharepapagh E, Dabiri S, Gilani N (2019) Correlation of cancer antigen 15-3 (CA15-3) serum level and bony metastases in breast cancer patients. Med J Islam Repub Iran 33:142. https://doi.org/10.34171/mjiri.33.142

Fu Y, Ma Q (2020) Recent developments in electrochemiluminescence nanosensors for cancer diagnosis applications. Nanoscale 12(26):13879–13898

Gerratana L, Fanotto V, Bonotto M, Bolzonello S, Minisini A, Fasola G, Puglisi F (2015) Pattern of metastasis and outcome in patients with breast cancer. Clin Exp Metasis 32:125–133

Graeser M, Schrading S, Gluz O, Strobel K, Herzog C, Umutlu L, Frydrychowicz A, Rjosk-Dendorfer D, Würstlein R, Culemann R (2021) Magnetic resonance imaging and ultrasound for prediction of residual tumor size in early breast cancer within the ADAPT subtrials. Breast Cancer Res 23(1):1–13

He Z-Y, Li X, Chen Q-S, Sun J-Y, Li F-Y, Wu S-G, Lin H-X (2016) Elevated serum carcinoembryonic antigen and CA15-3 levels and the risk of site-specific metastases in metastatic breast cancer. Transl Cancer Res 5(5):529–553

He F, Wang J, Yin B-C, Ye B-C (2018) Quantification of exosome based on a copper-mediated signal amplification strategy. Anal Chem 90(13):8072–8079

Hosseini SA, Mehri B, Niaei A, Izadkhah B, Alvarez-Galvan C, Fierro JGL (2018) Selective catalytic reduction of NOx by CO over $LaMnO_3$ nano perovskites prepared by microwave and ultrasound assisted sol–gel method. J Sol-Gel Sci Technol 85:647–656

Im H, Shao H, Park YI, Peterson VM, Castro CM, Weissleder R, Lee H (2014) Label-free detection and molecular profiling of exosomes with a nano-plasmonic sensor. Nat Biotechnol 32(5):490–495

Jia F-F, Zhong H, Zhang W-G, Li X-R, Wang G-Y, Song J, Cheng Z-P, Yin J-Z, Guo L-P (2015) A novel nonenzymatic ECL glucose sensor based on perovskite $LaTiO_3$–Ag0. 1 nanomaterials. Sens Actuators B Chem 212:174–182

Kodack DP, Askoxylakis V, Ferraro GB, Fukumura D, Jain RK (2015) Emerging strategies for treating brain metastases from breast cancer. Cancer Cell 27(2):163–175

Kowal J, Tkach M, Théry C (2014) Biogenesis and secretion of exosomes. Curr Opin Cell Biol 29:116–125

Lee TH, D'Asti E, Magnus N, Al-Nedawi K, Meehan B, Rak J (2011) Microvesicles as mediators of intercellular communication in cancer—the emerging science of cellular 'debris.' Seminars in immunopathology. Springer, Berlin, pp 455–467

Li C, Hu X, Lu J, Mao X, Xiang Y, Shu Y, Li G (2018) Design of DNA nanostructure-based interfacial probes for the electrochemical detection of nucleic acids directly in whole blood. Chem Sci 9(4):979–984

Lucas C, Eiroa I, Nunes M, Russo P, Ribeiro Carrott M, da Silva PM, Melo Jorge M (2009) Preparation and characterization of $Ca_{1-x} Ce_x MnO_3$ perovskite electrodes. J Solid State Electrochem 13:943–950

Luque GL, Ferreyra NF, Leyva AG, Rivas GA (2009) Characterization of carbon paste electrodes modified with manganese based perovskites-type oxides from the amperometric determination of hydrogen peroxide. Sens Actuators B Chem 142(1):331–336

Mahmoudi E, Mostafaei J, Griesser C, Bekheet MF, Delibas N, Penner S, Asghari E, Coruh A, Niaei A (2023) $LaCoO_3$–$BaCoO_3$ porous composites as efficient electrocatalyst for oxygen evolution reaction. Chem Eng J 473:144829

Mardi N, Haiaty S, Rahbarghazi R, Mobarak H, Milani M, Zarebkohan A, Nouri M (2023a) Exosomal transmission of viruses, a two-edged biological sword. Cell Commun Signal 21(1):1–29

Mardi N, Salahpour-Anarjan F, Nemati M, Baher NS, Rahbarghazi R, Zarebkohan A (2023b) Exosomes; multifaceted nanoplatform for targeting brain cancers. Cancer Lett 557:216077

Mobarak H, Heidarpour M, Rahbarghazi R, Nouri M, Mahdipour M (2021) Amniotic fluid-derived exosomes improved spermatogenesis in a rat model of azoospermia. Life Sci 274:119336. https://doi.org/10.1016/j.lfs.2021.119336

Mohammadi A, Farzi A, Thurner C, Klötzer B, Schwarz S, Bernardi J, Niaei A, Penner S (2022) Tailoring the metal-perovskite interface for promotional steering of the catalytic NO reduction by CO in the presence of H_2O on Pd-lanthanum iron manganite composites. Appl Catal B 307:121160

Mohseni SN, Majidi MR, Sohrabi H, Mahmoudi E, Delibas NC, Niaei A (2024) High-throughput screening of perovskite-based electrochemical sensor for determination of Piroxicam via electrocatalytic oxidation in pharmaceutical and biomedical analysis. Mater Chem Phys 316:129100

Molina R, Jo J, Filella X, Zanon G, Pahisa J, Muñoz M, Farrus B, Latre ML, Escriche C, Estape J (1998) c-erbB-2 oncoprotein, CEA, and CA 15.3 in patients with breast cancer: prognostic value. Breast Cancer Res Treat 51:109–119

Molina R, Jo J, Filella X, Zanon G, Farrus B, Munoz M, Latre M, Pahisa J, Velasco M, Fernandez P (1999) C-erbB-2, CEA and CA 153 serum levels in the early diagnosis of recurrence of breast cancer patients. Anticancer Res 19(4A):2551–2555

Molina R, Augé JM, Escudero JM, Filella X, Zanon G, Pahisa J, Farrus B, Muñoz M, Velasco M (2010) Evaluation of tumor markers (HER-2/neu oncoprotein, CEA, and CA 15.3) in patients with locoregional breast cancer: prognostic value. Tumor Biol 31:171–180

Mostafazadeh M, Kahroba H, Haiaty S, TazeKand AP, Samadi N, Rahbarghazi R, Nouri M (2022) In vitro exosomal transfer of Nrf2 led to the oxaliplatin resistance in human colorectal cancer LS174T cells. Cell Biochem Funct 40(4):391–402

Moura SL, Martín CG, Martí M, Pividori MI (2020) Electrochemical immunosensing of nanovesicles as biomarkers for breast cancer. Biosens Bioelectron 150:111882

Moura SL, Pallarès-Rusiñol A, Sappia L, Martí M, Pividori MI (2022) The activity of alkaline phosphatase in breast cancer exosomes simplifies the biosensing design. Biosens Bioelectron 198:113826

Mustacchi G, Biganzoli L, Pronzato P, Montemurro F, Dambrosio M, Minelli M, Molteni L, Scaltriti L (2015) HER2-positive metastatic breast cancer: a changing scenario. Crit Rev Oncol Hematol 95(1):78–87

Nasrollahpour H, Mahdipour M, Isildak I, Rashidi M-R, Naseri A, Khalilzadeh B (2021) A highly sensitive electrochemilumi-nescence cytosensor for detection of SKBR-3 cells as metastatic breast cancer cell line: a constructive phase in early and precise diagnosis. Biosens Bioelectron 178:113023

Nasrollahpour H, Khalilzadeh B, Naseri A, Mamaghani S, Isildak I, Rashidi M-R (2023) Chitosan/luminol/AgNPs nanocom-posite for electrochemiluminescent determination of prostate-specific antigen. Microchim Acta 190(3):90

Neagu A-N, Whitham D, Buonanno E, Jenkins A, Alexa-Stratulat T, Tamba BI, Darie CC (2021) Proteomics and its applica-tions in breast cancer. Am J Cancer Res 11(9):4006

Nezhad PDK, Bekheet MF, Bonmassar N, Schlicker L, Gili A, Kamutzki F, Gurlo A, Doran A, Gao Y, Heggen M (2021) Mecha-nistic in situ insights into the formation, structural and catalytic aspects of the La_2NiO_4 intermediate phase in the dry reforming of methane over Ni-based perovskite catalysts. Appl Catal A 612:117984

Pena M, Fierro J (2001) Chemical structures and performance of perovskite oxides. Chem Rev 101(7):1981–2018

Redig AJ, McAllister SS (2013) Breast cancer as a systemic disease: a view of metastasis. J Intern Med 274(2):113–126

Ryu JM, Kang D, Cho J, Lee JE, Kim SW, Nam SJ, Lee SK, Kim YJ, Im Y-H, Ahn JS (2023) Prognostic impact of elevation of cancer antigen 15-3 (CA15-3) in patients with early breast cancer with normal serum CA15-3 level. J Breast Cancer 26(2):126

Siegel RL, Miller KD, Jemal A (2018) Cancer statistics, 2018. CA Cancer J Clin 68(1):7–30

Sohrabi H, Dezhakam E, Khataee A, Nozohouri E, Majidi MR, Mohseni N, Trofimov E, Yoon Y (2022a) Recent trends in layered double hydroxides based electrochemical and optical (bio) sensors for screening of emerging pharmaceuti-cal compounds. Environ Res 211:113068

Sohrabi H, Dezhakam E, Nozohouri E, Majidi MR, Orooji Y, Yoon Y, Khataee A (2022b) Advances in layered double hydrox-ide based labels for signal amplification in ultrasensitive electrochemical and optical affinity biosensors of glucose. Chemosphere 309:136633

Sölétormos G, Nielsen D, Schiøler V, Mouridsen H, Dombernowsky P (2004) Monitoring different stages of breast cancer using tumour markers CA 15-3, CEA and TPA. Eur J Cancer 40(4):481–486

Sonnenblick A, Piccart M (2015) Adjuvant systemic therapy in breast cancer: quo vadis? Ann Oncol 26(8):1629–1634

Stremersch S, Marro M, Pinchasik BE, Baatsen P, Hendrix A, De Smedt SC, Loza-Alvarez P, Skirtach AG, Raemdonck K, Braeckmans K (2016) Identification of individual exosome-like vesicles by surface enhanced raman spectroscopy. Small 12(24):3292–3301

Sturgeon CM, Duffy MJ, Stenman U-H, Lilja H, Brunner N, Chan DW, Babaian R, Bast RC Jr, Dowell B, Esteva FJ (2008) National academy of clinical biochemistry laboratory medicine practice guidelines for use of tumor markers in testicular, prostate, colorectal, breast, and ovarian cancers. Oxford University Press, Oxford

Tangutoori S, Baldwin P, Sridhar S (2015) PARP inhibitors: a new era of targeted therapy. Maturitas 81(1):5–9

Thurner CW, Bonmassar N, Winkler D, Haug L, Ploner K, Delir Kheyrollahi Nezhad P, Drexler X, Mohammadi A, van Aken PA, Kunze-Liebhäuser J (2022) Who does the job? How copper can replace noble metals in sustainable catalysis by the formation of copper-mixed oxide interfaces. ACS Catal 12(13):7696–7708

Tsvetkova Y, Kozhukharov V (2009) Synthesis and study of compositions of the La–Sr–Ti–O system for SOFCs anode development. Mater Des 30(1):206–209

Wang Y, Xu Y, Luo Y, Ding Y, Liu X, Huang A (2010) A novel sensitive nonenzymatic glucose sensor based on perovskite LaNi0. 5Ti0. 5O$_3$-modified carbon paste electrode. Sens Actuators B Chem 151(1):65–70

Wang Y-Z, Zhong H, Li X-M, Jia F-F, Shi Y-X, Zhang W-G, Cheng Z-P, Zhang L-L, Wang J-K (2013a) Perovskite LaTiO$_3$–Ag0. 2 nanomaterials for nonenzymatic glucose sensor with high performance. Biosens Bioelectron 48:56–60

Wang B, Gu S, Ding Y, Chu Y, Zhang Z, Ba X, Zhang Q, Li X (2013b) A novel route to prepare LaNiO$_3$ perovskite-type oxide nanofibers by electrospinning for glucose and hydrogen peroxide sensing. Analyst 138(1):362–367

Wang L, Li J, Feng M, Min L, Yang J, Yu S, Zhang Y, Hu X, Yang Z (2017) Perovskite-type calcium titanate nanoparticles as novel matrix for designing sensitive electrochemical biosensing. Biosens Bioelectron 96:220–226

Wang L, Yang Y, Liu Y, Ning L, Xiang Y, Li G (2019) Bridging exosome and liposome through zirconium–phosphate coordi-nation chemistry: a new method for exosome detection. Chem Commun 55(18):2708–2711

Xu L, Shoaie N, Jahanpeyma F, Zhao J, Azimzadeh M, Al KT (2020) Optical, electrochemical and electrical (nano) biosen-sors for detection of exosomes: a comprehensive overview. Biosens Bioelectron 161:112222

Yadav S, Boriachek K, Islam MN, Lobb R, Möller A, Hill MM, Hossain MSA, Nguyen NT, Shiddiky MJ (2017) An electrochemi-cal method for the detection of disease-specific exosomes. ChemElectroChem 4(4):967–971

Yoon JS, Lim Y-S, Choi BH, Hwang HJ (2014) Catalytic activity of perovskite-type doped La0. 08Sr0. 92Ti1−xMxO3−δ (M= Mn, Fe, and Co) oxides for methane oxidation. Int J Hydrog Energy 39(15):7955–7962

Zhu Q, Chai Y, Zhuo Y, Yuan R (2015) Ultrasensitive simultaneous detection of four biomarkers based on hybridization chain reaction and biotin–streptavidin signal amplification strategy. Biosens Bioelectron 68:42–48

Publisher's Note